



HAL
open science

Experimental and numerical highlighting of water vapor sorption hysteresis in the coupled heat and moisture transfers

M. Maaroufi, F. Bennai, Rafik Belarbi, K. Abahri

► **To cite this version:**

M. Maaroufi, F. Bennai, Rafik Belarbi, K. Abahri. Experimental and numerical highlighting of water vapor sorption hysteresis in the coupled heat and moisture transfers. *Journal of Building Engineering*, 2021, 40, pp.102321. 10.1016/j.jobbe.2021.102321 . hal-03195367

HAL Id: hal-03195367

<https://hal.science/hal-03195367>

Submitted on 10 Mar 2023

HAL is a multi-disciplinary open access archive for the deposit and dissemination of scientific research documents, whether they are published or not. The documents may come from teaching and research institutions in France or abroad, or from public or private research centers.

L'archive ouverte pluridisciplinaire **HAL**, est destinée au dépôt et à la diffusion de documents scientifiques de niveau recherche, publiés ou non, émanant des établissements d'enseignement et de recherche français ou étrangers, des laboratoires publics ou privés.



Distributed under a Creative Commons Attribution - NonCommercial 4.0 International License

1 **Experimental and numerical highlighting of water vapor sorption**
2 **hysteresis in the coupled heat and moisture transfers**

3 M. Maaroufi^{1,2}, F. Bennai⁴, R. Belarbi^{2,3*}, K. Abahri¹

4 ¹ LMT, ENS Paris-Saclay, CNRS, Université Paris-Saclay, 61 avenue du Président Wilson, 94235
5 Cachan, France

6 ² University of La Rochelle, CNRS, LaSIE UMR 7356, Avenue Michel Crépeau, 17042 La Rochelle
7 Cedex 1, France

8 ³ 4ev Lab, EDF R&D, CNRS, LaSIE, Université de La Rochelle, Avenue Michel Crépeau 17042 La
9 Rochelle cedex1, France

10 ⁴ Université de Lorraine, CNRS, Arts et Métiers ParisTech, LEM3, F-57000, Metz, France

11 *Corresponding author: Rafik Belarbi

12 Email address: rbelarbi@univ-lr.fr

13 Phone Number: +33 (0)5 46 45 72 39

14 Postal Address : LaSIE, La Rochelle Université, Avenue Michel CREPEAU 17042, La Rochelle
15 Cedex 1, France

16

17 **Highlights**

18 - Experimental and numerical study of water vapor sorption hysteresis.

19 - Development of a coupled heat and mass transfer model with consideration of sorption
20 hysteresis.

21 - Sorption hysteresis model allows a better adequacy of simulated results with experimental
22 ones.

23 - Non-hysteresis model shows various discrepancies and relative gaps between experimental
24 and numerical results reached 28%.

25 **Abstract**

26 Heat, air and moisture transfers have a significant influence on indoor ambience and
27 affect both temperature and hygrometry values and energy performance of buildings.
28 Furthermore, high levels of humidity may lead to severe pathologies in building walls in
29 addition to tamper indoor air quality and hygrothermal comfort. Sorption hysteresis
30 phenomenon is responsible for the moisture accumulation in porous building materials, and
31 leaving it out in hygrothermal modelling would result in an incorrect water content value.

32 The present work aims to highlight the influence of the sorption hysteresis
33 phenomenon on heat and moisture transfer in expanded polystyrene concrete. In order to
34 achieve this, a coupled heat and mass transfer model will be elaborated, taking consideration
35 of sorption hysteresis phenomenon. Experimental protocols will be conducted to highlight the
36 hysteresis in the materials, and the results will be compared to those of the numerical
37 simulations. A simple hygrothermal transfer model without including hysteresis will also be
38 used in the numerical simulations so that it is compared to the developed model. Experimental
39 results show that considering the hysteresis phenomenon allows to better apprehend the
40 hygrothermal behavior of building materials, and neglecting it leads to important differences
41 sometimes reaching 28%.

42 **Key words**

43 Sorption hysteresis; Coupled heat and moisture transfers; Hygrothermal modelling;
44 Experimental characterization; Numerical simulations.

45 **List of symbols**

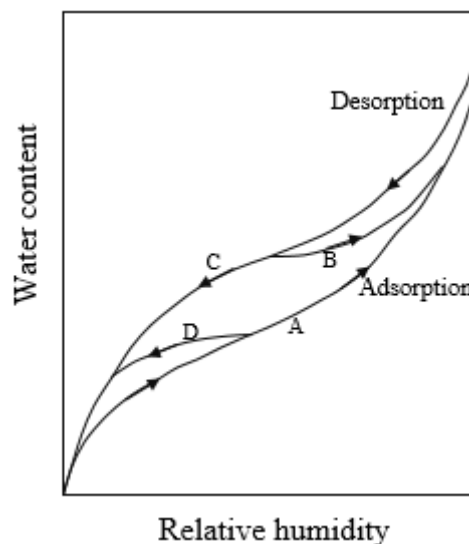
U: Volume water content (kg/m ³)	RH: Relative humidity (%)
ω : Mass water content (kg/kg)	P_{vsat} : Saturation vapor pressure (Pa)
U_v : Water vapor content (kg/m ³)	ρ_s : Density (kg/m ³)
U_l : Liquid water content (kg/m ³)	K_m : Moisture diffusion coefficient (kg/m.s)
m: phase change ratio	δ_a : Water vapor permeability of air (kg/m.s.Pa)
j_v : Water vapor flux density (kg/m ² .s)	μ : Water vapor diffusion resistance
j_l : Liquid water flux density (kg/m ² .s)	H: Enthalpy (J/kg)
j_m : Total mass flux (kg/m ² .s)	ϕ : Total heat flux (W/m ²)
δ_v : Water vapor permeability (kg/m.s.Pa)	ψ : Internal energy (J)
δ_l : Liquid water permeability (kg/m.s.Pa)	C_p : Specific heat (J/g.K)
P_v : Water vapor pressure (Pa)	λ : Thermal conductivity (W/m.K)
P_c : Capillary pressure (Pa)	L_v : Latent heat of vaporization (J/kg)
C_{pv} : Specific heat of water vapor (J/g.K)	R: Gaz constant (J/K.mol)
T : Temperature (K)	M : Molar mass (kg/mol)

46 **1. Introduction**

47 Indoor air humidity is as important as indoor air temperature, since moisture can
 48 significantly influence the energy performance of households [1,2], and is one of the main
 49 causes of its deterioration [3,4]. Moisture in porous building materials can also greatly affect
 50 the indoor air quality and comfort of occupants, given that excessive low or high humidity can
 51 cause multiple respiratory pathologies and allergies [5]. To predict those effects, moisture
 52 transfer has been studied for a long time, especially in unsaturated porous media based on
 53 Darcy and Fick's laws [6,7]. To avoid moisture condensation, insulation failure or mold

54 growth in building materials, coupled heat and moisture transfers should be studied together
55 for a better prediction of the hygrothermal behavior of the building, and thus optimize its
56 design [8 – 10]. Hygrothermal transfers are often expressed using mainly phenomenological
57 models [11,12] or models that consider the materials microstructure through porosity or pore
58 size distribution [13,14].

59 Adsorption and desorption isotherms are among the most important hydric properties
60 of porous building materials, since they describe the equilibrium water content as a function
61 of the ambient relative humidity, at a certain temperature. Cement based materials often
62 exhibit a hysteresis loop, meaning the moisture content at the same relative humidity is
63 different whether the material experiences wetting or drying. Therefore, the moisture content
64 also depends on the hydric history of the material [15], and the water content follows the
65 intermediate scanning curves (fig.1, curves B and D) located between the two main adsorption
66 and desorption curves (fig.1, curves A and C) [16].



67

68 **Fig.1** Sorption hysteresis curves [17]

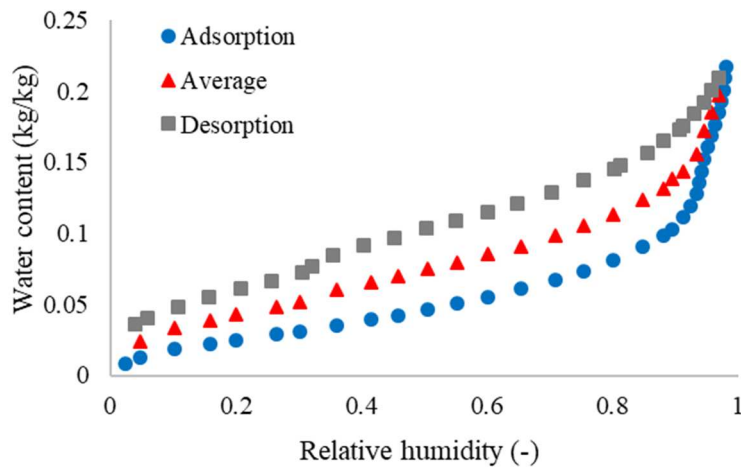
69 Sorption hysteresis should then be taken into consideration in any hygrothermal
70 transfers research, since it illustrates the fact that it is easier for water to get in than to get out

71 of a porous medium [18] and is highly correlated to capillary forces [19]. In the past few
72 decades, the interest about this phenomenon has highly increased, and researchers began
73 developing hygrothermal models considering the effect of sorption hysteresis. However, it
74 remains unknown and less studied in the literature, unlike other conventional phenomena such
75 as hydration or carbonation.

76 Some researches exhibited sorption hysteresis experimentally and considered it in the
77 heat and mass transfers modelling. In his work, Zhang [20] studied cement pastes initially
78 saturated, then subjected to hydric cycles varying from 33% to 80% and finally 53,5% of
79 relative humidity. He then validated his hygrothermal model using experimental saturation
80 profiles. However, he only subjected the samples to only one cycle of wetting and drying,
81 which is not representative of buildings. Ait Oumeziane [21] also studied sorption hysteresis
82 phenomenon in a hemp concrete, a very hygroscopic material. Samples were subjected to
83 many cycles of 75% of relative humidity during 8h, then 33% during 16h, corresponding to
84 the NORDTEST protocol for the determination of Moisture Buffer Value [22]. However,
85 some input parameters were only taken from literature and not measured for the studied
86 material, and thermal conductivity dependency was modeled based on its values at the dry and
87 saturated state only. The evolution of the water content in the material was compared to
88 numerical simulations. In line with this work, Lelièvre [23] also studied hysteresis in hemp
89 concrete through three different experimentations. The difference lies in the duration of the
90 relative humidity levels, which varies from few hours to few days. Nevertheless, thermal
91 properties of the material were considered constant regardless of its water content, and most
92 of the input parameters were taken from previous works in literature.

93 Other researches designed sorption hysteresis modelling using a physical approach,
94 based on the microstructure of the materials. Schiller et al. [24] recently proposed a hysteresis
95 model in hardened cement pastes with consideration of the sorption in the interlayer space

106 between the C-S-H sheets, which is supposed to be responsible for low-pressure hysteresis of
107 water sorption isotherms. Their work is based on a macroscopic approach using a simple
108 mathematical model coupled to volume change diagrams. Only computed hysteresis loops
109 were compared to those observed experimentally. Jiang et al. [25] developed a model to
110 predict water vapor sorption hysteresis of cement-based materials based on pore size
111 distribution obtained from adsorption isotherms. No suited experimental campaign was led to
112 validate the model, which was verified using water vapor sorption isotherms from literature.
113 However, sorption isotherms are determined at equilibrium, while materials in buildings
114 undergo dynamic humidity variations.



105

106

Fig.2 Main and average sorption curves for hemp concrete [26]

107

108

109

110

111

112

113

114

In most of the numerical studies of hygrothermal transfers, sorption hysteresis is often neglected. Some works prefer to overestimate the water content and consider that it varies according to the evolution of the main desorption curve for each variation of the daily relative humidity, whether it is a wetting or a drying [27 – 29]. Some researchers assume that the water content rather follows the path of the main adsorption curve and do not consider sorption hysteresis [18], and others even consider a mean curve between the main sorption isotherms, introducing some weighting coefficients [20]. These choices are difficult to justify, given that water content in a porous material follows different paths whether it is subjected to

115 a wetting or drying. In fact, at the same relative humidity, water content has two different
116 values, and the relative gap between them is very high. In the case of very hygroscopic
117 materials such as hemp concrete [26], the difference can go from 50% to 100%, as shown in
118 figure 2.

119 The water content depends then on the relative humidity of the environment in
120 addition to the previous hydric states of the material. Therefore, sorption hysteresis must be
121 taken into account in the modelling of coupled heat and mass transfers in building materials,
122 because it allows determining a more precise value of water content at any given time.

123 In this context, we propose a hygrothermal transfer model considering the sorption
124 hysteresis phenomenon using the sorption isotherms. The heat and mass transfer model is
125 based on Luikov's equations [30], including some improvements in the hypotheses. Indeed,
126 input parameters were not supposed constant, and their temperature and water content
127 dependency were considered. Sorption hysteresis phenomenon is also considered, and an
128 adequate experimental campaign was carried on in order to validate the computed results.
129 Moreover, in order to reduce the environmental footprint of building sector, a recycled
130 expanded polystyrene mortar will be the material of interest. It is an eco-friendly material that
131 helps reuse the expanded polystyrene waste and has improved thermal insulation properties. It
132 is a highly heterogeneous material with a complex microstructure, and is composed of two
133 materials whose hygrothermal behavior highly varies.

134 In what follows, the hygrothermal model will be presented, along with its
135 implementation on Matlab and Comsol multiphysics. The experimental setup allowing the
136 highlight of hysteresis will be presented, and the obtained results will be compared to the ones
137 from the numerical calculations using the hysteresis model. A non-hysteresis model will also
138 be used in order to enhance the influence of the sorption hysteresis phenomenon. It is

139 implemented using the main adsorption isotherm only, and it aims to show the importance of
140 sorption hysteresis consideration in hygrothermal transfers modelling.

141 **2. Modelling**

142 **2.1. Heat and mass transfers modelling**

143 In this study, the implemented model is a coupled heat and mass transfers model using
144 respectively temperature and water content as driving potentials. Afterwards, it will be
145 coupled to a physical model that allows calculating the water content inside the pores from the
146 ambient relative humidity with the consideration of sorption hysteresis.

147 The mass balance equations for the water vapor and liquid water phases respectively are
148 written below:

$$149 \quad \frac{\partial U_v}{\partial t} + \text{div}(j_v) = -m \quad (1)$$

$$150 \quad \frac{\partial U_l}{\partial t} + \text{div}(j_l) = m \quad (2)$$

151 By adding the two equations, we obtain the equation (3) that simplifies into equation (4).

$$152 \quad \frac{\partial U_v}{\partial t} + \frac{\partial U_l}{\partial t} + \text{div}(j_v) + \text{div}(j_l) = 0 \quad (3)$$

$$153 \quad \frac{\partial U}{\partial t} + \text{div}(j_v + j_l) = 0 \quad (4)$$

154 Given that the volume water content is function of the mass water content and the materials
155 density (equation (5)), the mass balance equation becomes equation (6).

$$156 \quad U = \rho_s \times \omega \quad (5)$$

$$157 \quad \rho_s \frac{\partial \omega}{\partial t} + \text{div}(j_v + j_l) = 0 \quad (6)$$

158 Flux densities of water vapor and liquid water can be expressed using adequate diffusion
159 coefficients, which depend on the hydric state of the material as:

160
$$j_v = -\delta_v \cdot \nabla P_v \quad (7)$$

161
$$j_l = -\delta_l \cdot \nabla P_c \quad (8)$$

162 In order to simplify the boundary conditions, water vapor content is considered the only
 163 driving force of the mass transfers. Moreover, both the water vapor pressure and the capillary
 164 pressure are related to relative humidity through the saturated vapor pressure and Kelvin law.

165
$$P_v = RH \times P_{vsat} \quad (9)$$

166
$$P_c = \frac{RT\rho_l}{M} \ln(RH) \quad (10)$$

167 Given the dependency of relative humidity on the temperature, the derivative of equation (10)
 168 is expressed as follows [31]:

169
$$\nabla P_c = \left[\frac{RT\rho_l}{M} \frac{1}{RH} \nabla RH \right] + \left[\frac{RT\rho_l}{M} \left(\frac{\partial \ln(RH)}{\partial T} \right) + \frac{R\rho_l}{M} \ln(RH) \right] \nabla T \quad (11)$$

170 The thermal diffusion is negligibly small, and considered of no importance in building science
 171 applications [32,33]. Therefore, the total mass flux can be expressed in the equation (12).

172
$$j_m = - \left[\delta_v P_{vsat} + \delta_l \frac{RT\rho_l}{M} \frac{1}{RH} \right] \nabla RH \quad (12)$$

173 The moisture storage capacity C_m is defined as the slope of the sorption isotherm curves [34].
 174 It is then a function of relative humidity and water content. It is an important property of the
 175 material as it represents the water accumulation in the pores due to sorption hysteresis.

176
$$C_m = \frac{\partial \omega}{\partial RH} \quad (13)$$

177 The final expression of the mass balance equation is then explicated in equation (14).

178
$$\rho_s \frac{\partial \omega}{\partial t} - \text{div} \left[\frac{K_m}{C_m} (\nabla \omega) + \frac{\delta_l}{C_m} \frac{R \cdot T_{ref} \cdot \rho_l}{M \cdot RH} (\nabla \omega) \right] = 0 \quad (14)$$

179 We set $K_l = \frac{\delta_l}{C_m} \frac{R \cdot T_{ref} \cdot \rho_l}{M \cdot RH}$ to simplify the mass balance equation.

180
$$\rho_s \frac{\partial \omega}{\partial t} - \text{div} \left[\frac{K_m}{C_m} (\nabla \omega) + K_l (\nabla \omega) \right] = 0 \quad (15)$$

181 The moisture diffusion coefficient that appeared in the mass balance equation is defined as
 182 below [23, 35, 36]:

183
$$K_m(\omega) = \frac{\delta_a}{\mu(\omega)} P_{\text{vsat}} = \delta_v(\omega) P_{\text{vsat}} \quad (16)$$

184 The heat balance equation is expressed in the equation (17) [36]. We only consider heat
 185 transfers due to conduction, convection and phase change, and we neglect the radiation
 186 phenomenon. The final conservation of energy equation is then as:

187
$$C_p \rho_s \frac{\partial T}{\partial t} - \text{div}(\lambda \nabla T) - K_m C_{pv} \nabla T - m L_v \omega = 0 \quad (17)$$

188 **2.2. Initial and boundary conditions**

189 The boundary conditions in this paper are Dirichlet type, and the temperatures and relative
 190 humidities are directly applied to the exterior surfaces of the sample.

191
$$\begin{cases} \omega(x=0, t) = \omega_1(t) \\ T(x=0, t) = T_1 \end{cases} \quad \text{and} \quad \begin{cases} \omega(x=L, t) = \omega_2(t) \\ T(x=L, t) = T_2 \end{cases} \quad (18)$$

192 Where L is the thickness of the sample. The initial conditions are considered uniform in the
 193 material and expressed as follows:

194
$$\begin{cases} \omega(x, t=0) = \omega_0 \\ T(x, t=0) = T_0 \end{cases} \quad (19)$$

195 **2.3. Input parameters**

196 The input parameters of the heat and mass transfers model are the hygrothermal properties of
 197 the material, that were determined using an experimental campaign. The moisture storage
 198 capacity C_m is obtained through the water vapor sorption isotherm curves presented later.

199 The thermal conductivity of the material depends on the temperature and the water content of
 200 the material, and it was experimentally determined based on the guarded hot plate method
 201 [37]. The thermal conductivity of the polystyrene mortar can be expressed as a function of
 202 temperature as follows:

$$203 \quad \lambda = 0,0005 \cdot T + 0,1472 \quad (20)$$

204 The thermal conductivity was also measured depending on the hydric state of the material. Its
 205 dependency on the water content is expressed in equation 21.

$$206 \quad \lambda = 0,3663 \cdot \omega + 0,1413 \quad (21)$$

207 The water vapor permeability of polystyrene concrete depends on the materials water content,
 208 and it was experimentally determined following the cup test method based on the standards
 209 NF EN ISO 12572 [38]. This method allows determining the water vapor permeability at a
 210 low and a high relative humidity (3% and 93%). Hence, water vapor permeability will have
 211 two different values whether the ambient relative humidity is high or low.

ρ_s (kg/m ³)	537	C_p (J/kg.K)	971
T _{ref} (K)	273,15	C_{pv} (J/kg.K)	1860
δ_v (kg/m.s.Pa)	3,22.10 ⁻¹² at low RH 1,2.10 ⁻¹¹ at high RH	m (-)	0,3
L_v (J/kg)	2,5.10 ⁶		

212 **Table 1.** Input parameters

213 **2.4. Sorption hysteresis modelling**

214 The coupled heat and mass transfers model will be coupled to a sorption hysteresis
 215 model. Therefore, in addition to taking into account the moisture accumulation inside the
 216 pores through the moisture storage capacity, it will be able to calculate the real value of water

217 content from the ambient relative humidity. The sorption hysteresis model chosen for this
218 work is the one developed by Carmeliet [39], which is a physical model based on the theory
219 of the independent domains and the ink-bottle pore effect, elaborated by Mualem [40,41]. In
220 previous works, this model was proven to be the most representative to the hysteretic behavior
221 of cement based materials [21,23].

222 The use of empirical hysteresis models often leads to a hysteretic behavior called
223 "pumping effect". It reflects the fact that the numerical scanning curves do not respect the
224 closing principle. In other words, this means that during a succession of adsorption and
225 desorption cycles, there is a unique water content value for each extremum of relative
226 humidity. Therefore, a material undergoing several cycles of wetting /drying should normally
227 return to its initial relative humidity and water content.

228 Some researches [20,42,43] consider that the pumping effect is not a physical
229 characteristic specific to the material, but that it is entirely artificial. It is then considered as
230 errors generated by the calculation algorithms. Mualem model – and therefore Carmeliet
231 model – respects the closing principle and makes it possible to avoid pumping errors,
232 confirming its accuracy in hysteresis modelling [29,23].

233 The sorption hysteresis model developed by Carmeliet allows calculating modelled
234 hysteresis loops from the main adsorption and desorption isotherm curves. It is based on the
235 theory of independent domains, considering the ink-bottle shaped pores. It expresses the water
236 content in the scanning curves in different expressions, whether it is a wetting or a drying, in
237 terms of water content in the main sorption isotherms, and some specific values such as
238 saturation point.

239 The equation describing the water content in adsorption scanning curves is recalled below.

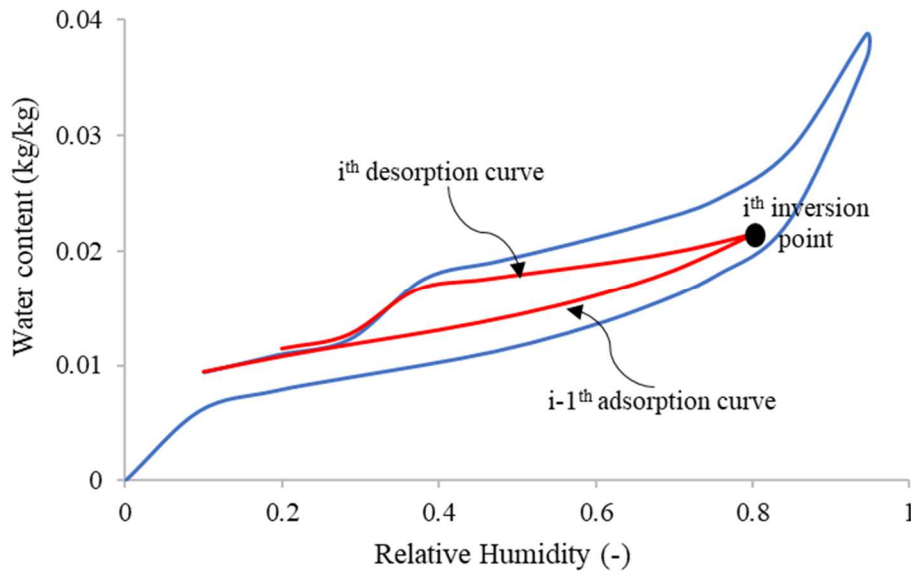
$$240 \quad \omega_{\text{ads,hyst}}(\text{RH}, i) = \omega_{i-1} + (1 - A(\text{RH}_{i-1}))(\omega_{\text{ads}}(\text{RH}) - \omega_{\text{ads}}(\text{RH}_{i-1})). \quad (22)$$

241 The “i” indicates the inversion point which is the exact time of going from an
 242 adsorption to a desorption (and vice versa). In equation (22), the “i” here marks the inversion
 243 between the $i-1^{\text{th}}$ desorption scanning curve and the i^{th} adsorption scanning curve.

244 The equation describing the water content in desorption scanning curves is expressed
 245 in (23). In this case, the “i” marks the inversion between the $i-1^{\text{th}}$ adsorption scanning curve
 246 and the i^{th} desorption scanning curve, as explicated in figure 3.

$$247 \quad \omega_{\text{des,hyst}}(\text{RH}, i) = \omega_{i-1} - (1 - A(\text{RH}))(\omega_{\text{ads}}(\text{RH}_{i-1}) - \omega_{\text{ads}}(\text{RH})), \quad (23)$$

$$248 \quad \text{Where} \quad A(\text{RH}) = \frac{\omega_{\text{des}}(\text{RH}) - \omega_{\text{ads}}(\text{RH})}{\omega_{\text{sat}} - \omega_{\text{ads}}(\text{RH})} \quad (24)$$



249

250 **Fig.3** Schematic representation of the i^{th} inversion point

251 The water content associated to each varying value of relative humidity is calculated
 252 whether it is a wetting or a drying. For that, we need to know and memorize the inversion
 253 points. It is then necessary to indicate a transition criterion between the different phases of
 254 wetting/drying, along with a list of the inversion points [21]. Equation (25) expresses the
 255 condition of the transition from the adsorption curve to the desorption curve, and vice versa.

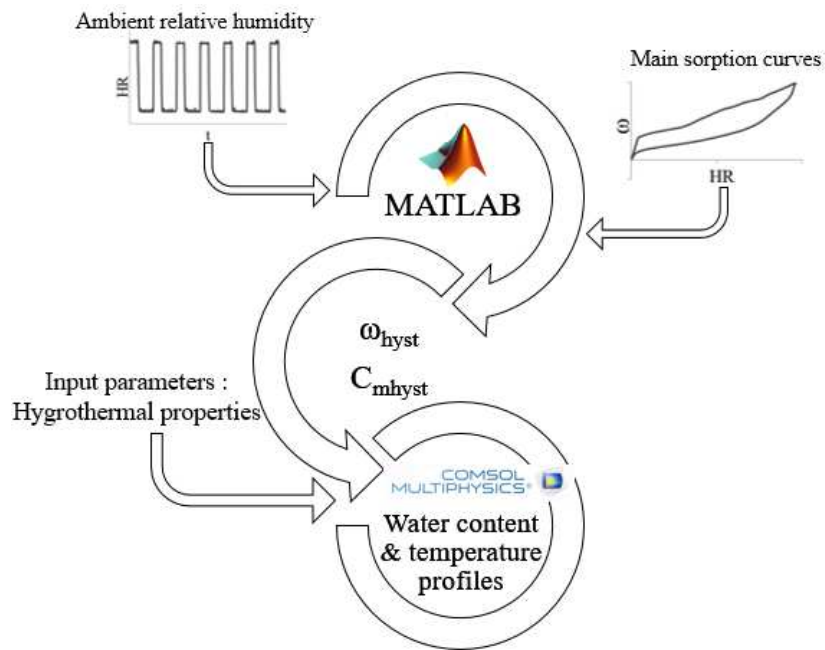
256 When the inversion criterion is less than zero, there is a transition from a sorption phase to the
257 other, and the new inversion point is added to the list.

$$258 \quad L_{inv} = (RH(n) - RH(n - 1)) \times (RH(n - 1) - RH_{i-1}) \quad (25)$$

259 $RH(n)$ represents the relative humidity of the material at the time n , $RH(n-1)$ at the
260 time $n-1$, and RH_{i-1} corresponds to the relative humidity of the last identified inversion point.
261 The iterations in the program stand for the time. There is an inversion if the inversion criterion
262 is less than zero. In this case, this new point is saved and becomes the last identified inversion
263 point. The values of relative humidity and water content are therefore calculated at each time,
264 and the water capacity is calculated differently whether it is an adsorption or a desorption.

265 As shown in figure 4, MATLAB software was used to compute the hysteresis model,
266 coupled to COMSOL Multiphysics where the hygrothermal model was implemented. The
267 experimental values of ambient relative humidity and the main adsorption and desorption
268 curves are first introduced in MATLAB where the hysteresis model allows the calculation of
269 the corresponding values of water content, in addition to the moisture storage capacity. These
270 values are then imported into COMSOL along with the input parameters consisting in the
271 hygrothermal properties of the material of interest. The resolution in Comsol is based on the
272 finite elements method following three basic steps, namely pre-processing, solver, and post-
273 processing. It generates a set of equations for all the involved physical models and
274 implements them in a single iteration scheme, which is repeated until convergence is reached.
275 Comsol has several solvers all based on finite elements method, then chooses the most
276 suitable one to ensure stability and convergence of the solutions. The time dependent solver is
277 computing the solution to a possibly nonlinear system of equations at each time step via a set
278 of iterative techniques based upon Newton's method. These Newton's method techniques for
279 solving a nonlinear system of equations evaluate a function, as well as its derivative, at every

280 time step. This derivative is also known as the Jacobian and is relatively expensive to
 281 compute. Therefore, the software will try to minimize reevaluating the Jacobian, by default. If
 282 the nonlinear solver has difficulty converging, it will reduce the requested time step size and
 283 try to compute the solution.



284

285

Fig.4 Hysteresis modelling steps

286

3. Materials and methods

287

288

289

290

291

292

293

294

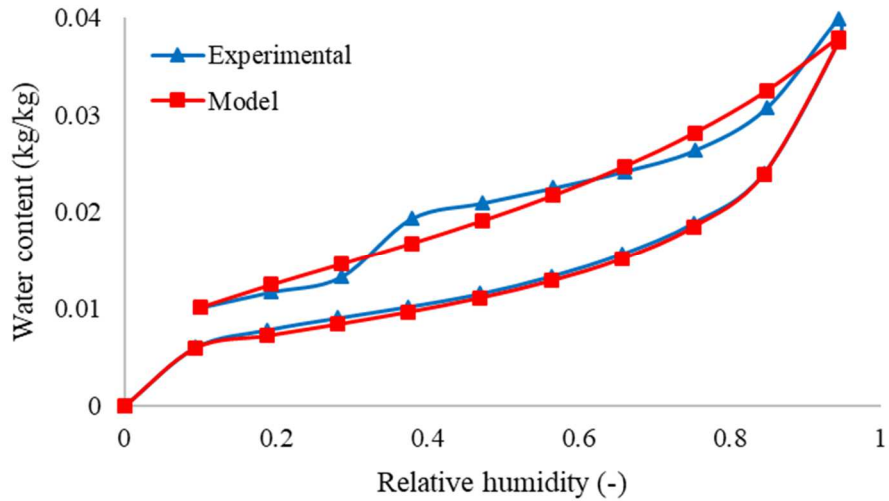
In this study, the coupled heat and moisture transfers model developed is based on phenomenological modelling, where the relevance of the prediction is conditioned by a reliable evaluation of the input data. The hygrothermal properties that constitute the input parameters of the implemented model were experimentally determined using standard laboratory methods. A part of this section was dedicated to a fine, experimental characterization of the intrinsic hydric and thermal properties of the material. The material of interest in this work is a polystyrene mortar made of recycled expanded polystyrene granules and a CEMII cement as a binder [44,45].

295 Computing the coupled heat and mass transfers involves the experimental
296 determination of the hygrothermal properties of the material. The experimental campaign
297 aimed to measure the water vapor permeability using the wet cup/dry cup method based on
298 the EN ISO 12572 norm [46], the thermal conductivity using the Guarded Hot Plate method
299 based on the NF EN 12667 norm [47], and the heat capacity using a 3D sensors calorimeter.

300 In addition, the implementation of the hysteresis model requires the determination and
301 modelling of the main adsorption and desorption curves of the material. The experimental
302 isotherm curves were determined using the gravimetric technique that is based on continuous
303 successive weightings. The test was performed on a very recent vapor sorption analyzer that
304 allows measuring the mass evolution of the samples. For the polystyrene mortar, the main
305 isotherms are modelled using the equation below [39], which proves a good adequacy
306 between the experimental and the modelled curves, as shown in figure 5.

$$307 \quad \omega(\text{RH}) = \omega_{\text{sat}} \left(1 - \frac{\ln(\text{RH})}{A} \right)^{-1/n} \quad (26)$$

308 A and n are empirical calibration coefficients. These parameters were adjusted using the
309 experimental data presented in figure 5. The fitting parameters are presented in table 2, and
310 are different whether it is adsorption or desorption. The root mean squared error between the
311 experimental data and the adjustment curves is 0,2%.



312

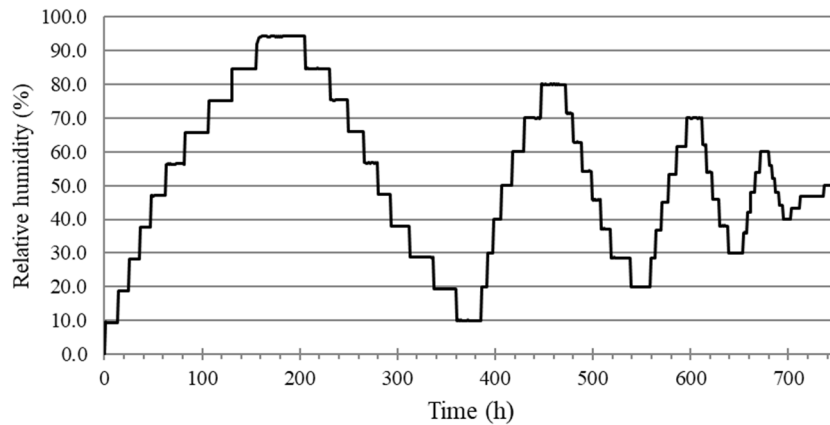
313 **Fig.5** Main adsorption and desorption isotherm curves of polystyrene mortar

314 This model precisely reproduces the sorption isotherms of the polystyrene mortar in
 315 adsorption phase, and is less accurate in desorption phase. This is due to the sudden decrease
 316 of water content in the main desorption curve between 30% and 40% of relative humidity,
 317 that is very difficult to model.

	A	n	R ²
Adsorption	0,033	1,796	0,996
Desorption	0,399	1,35	0,965

318 **Table 2.** Fitting coefficients for the main sorption isotherms

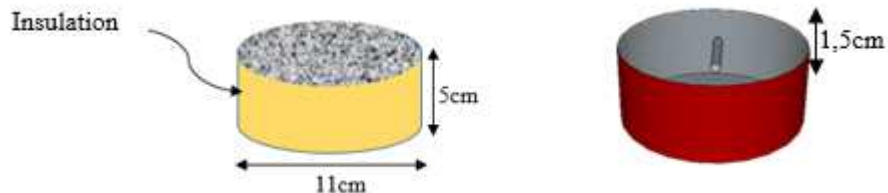
319 During the daily variations of relative humidity and temperature, the water content
 320 inside building materials varies according to the intermediate sorption isotherms. In order to
 321 characterize experimentally the intermediate curves of the expanded polystyrene mortar, the
 322 total water content is measured at the equilibrium when subjecting the material to different
 323 relative humidity levels. The experimental method used here was the gravimetric technique
 324 that is based on continuous successive weightings. The test was performed on three cubic
 325 samples of 10x10x10 mm³ dimensions previously dried at 60°C. The temperature was fixed at
 326 23°C and the relative humidity variations are presented in figure 6.



327

328 **Fig.6** Relative humidity variation during the determination of the intermediate isotherms

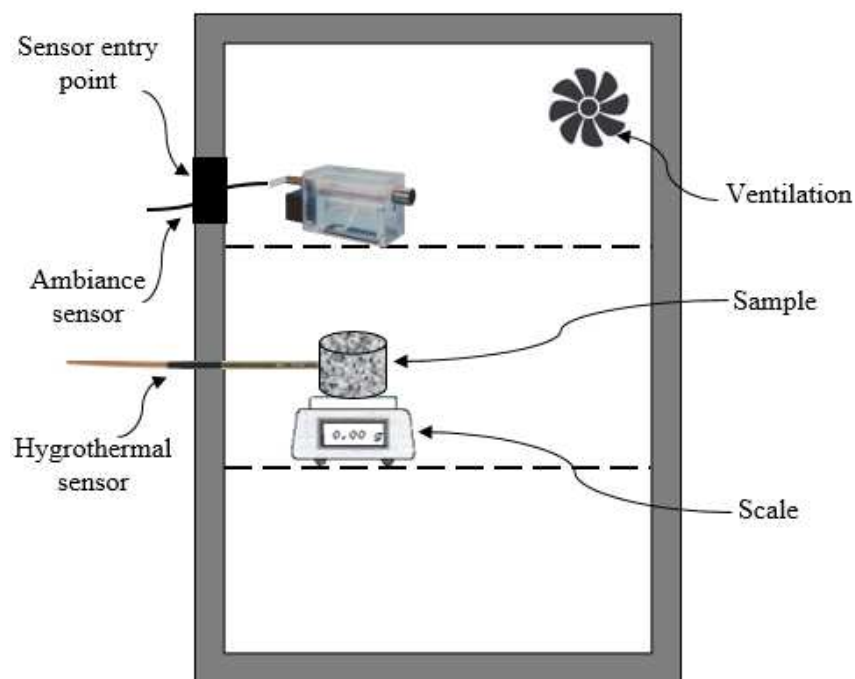
329 A second experimental campaign dedicated to the validation of the model was
 330 performed. The objective is to assess the relevance of the coupled heat and moisture transfers
 331 model by confronting it to experimental results on the one hand, and on the other hand to
 332 highlight the influence of considering the hysteresis of water content in the developed model.
 333 The experimentation consists of imposing a unidirectional transfer through cylindrical
 334 samples by applying a thermal and hydric insulation on all the surfaces but one, as
 335 schematized in figure 6. Hygrothermal sensors are introduced inside the samples in order to
 336 record the temperature and relative humidity evolution. The sensors were positioned 1,5cm
 337 away from the surface of the sample, as shown in figure 7. The samples were then be
 338 subjected to cyclic solicitations in temperature and relative humidity applied on the exposed
 339 surface. Samples are initially conditioned at 50% of RH and 25°C.



340

341 **Fig.7** Samples dimensions (left) and sensors disposition (right)

342 The experimental setup is presented in figure 8, and is composed of a climatic
343 chamber in charge of the ambient conditions and a high accuracy ambience sensor ensuring
344 compliance with the ambient conditions imposed on the sample in terms of temperature and
345 relative humidity. High precision sensors are also put inside the samples in order to obtain the
346 temperature and water content profiles at different positions in the material. Each sample is
347 put on a scale so that it can measure the total water content during the experimentation. The
348 climatic chamber is of type Memmert HCP240 and the ambience sensor is a psychrometer of
349 high precision ($\pm 1\%$ in the whole relative humidity range). The hygrothermal sensors used
350 inside the samples are capacitive humidity sensors FHA 646 R, characterized by $\pm 2\%$ of
351 precision in relative humidity range and $\pm 0,2\text{K}$ for a temperature from 0 to 70°C.



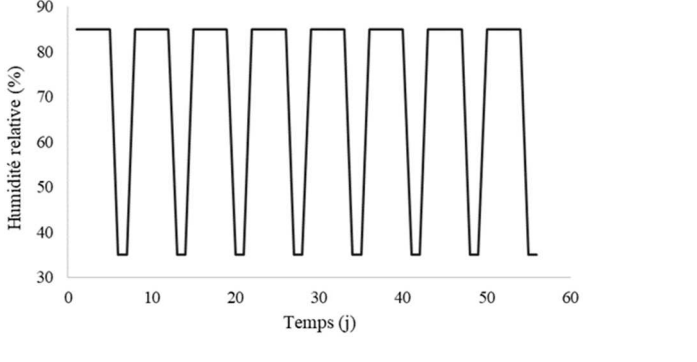
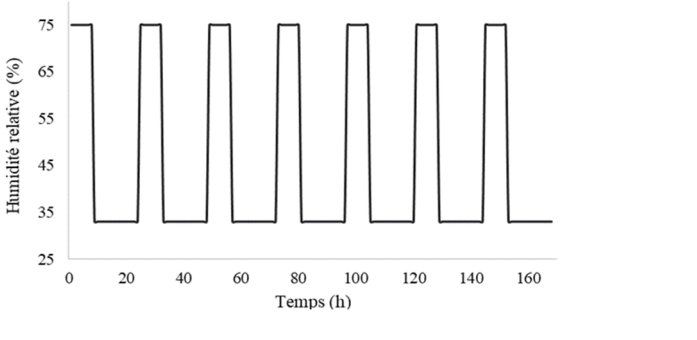
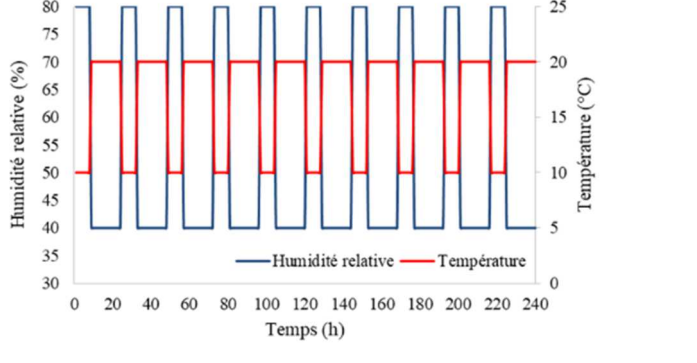
352

353

Fig.8 Experimental setup diagram

354 For us, to study the materials response to long and short cyclic solicitations, three
355 different hygrothermal conditions were tested. The first protocol is set in a way to consider
356 the reaction of the material to hydric solicitations with low drying kinetics, at a constant
357 temperature. The two other protocols aim to simulate the daily variations of climatic

358 conditions, but one is at a constant temperature, and in the other one it varies along with the
 359 relative humidity. The detailed solicitations and their durations are presented in table 3.

<p>Long-lasting cycles at constant temperature</p>	<p>8 cycles 85% RH for 5 days 35% RH for 2 days T = 23°C</p>	
<p>Short-lasting cycles at constant temperature</p>	<p>7 cycles 75% RH for 8h 33% RH for 16h T = 25°C</p>	
<p>Short-lasting cycles at varying temperature</p>	<p>10 cycles 80% RH for 8h at 10°C 40% RH for 16h at 20°C.</p>	

360 **Table 3.** Experimental hydric and thermal conditions

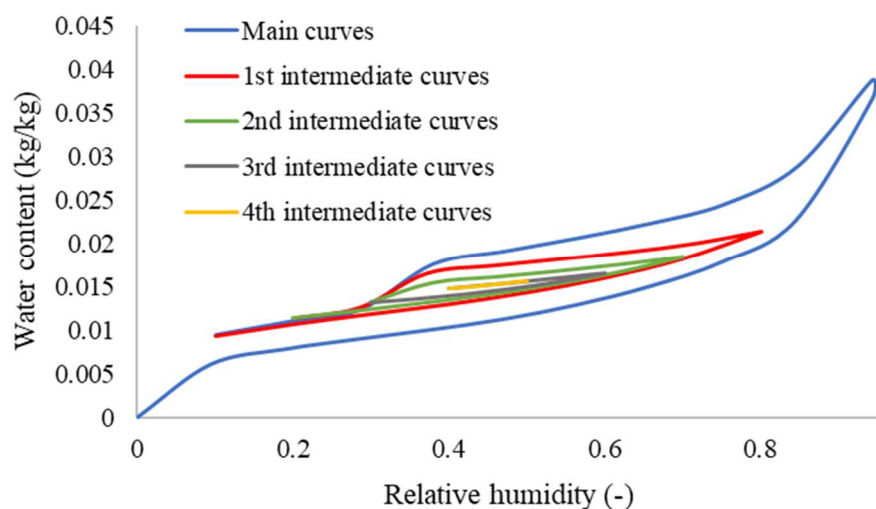
361 **4. Results and discussion**

362 In the following, the experimental and numerical results are presented. First, the
 363 intermediate adsorption and desorption curves of the polystyrene mortar are presented, in
 364 addition to the experimental and modelled moisture storage capacity curve. Afterwards, the
 365 experimental water content profiles inside the samples, along with the simulated water content
 366 profiles are presented simultaneously in order to compare both. The three different

367 experimental protocols presented in table 3 are treated separately, in order to compare
368 between the experimental and simulated profiles in each case.

369 4.1. Main and intermediate sorption curves

370 The experimental adsorption and desorption curves of the polystyrene mortar are
371 presented in the figure 9. Given that the sample was initially at a dry state, the first curves are
372 the main adsorption and desorption isotherms, while all the others represent the intermediate
373 curves. The scanning curves are all located between the main curves, which represent an
374 envelope curve. They have the same look and vary in the same way, they even present the
375 abrupt decrease in desorption around 30% of relative humidity. After four cycles of the
376 wetting and drying cycles presented in figure 6, the intermediate curves overlap, thus the 4th
377 adsorption curve and the 3rd desorption curve are imbricating. These results come from the
378 water accumulation in the materials porosity and the sorption hysteresis phenomenon, since
379 the relative humidity conditions are narrowed down after each cycle.

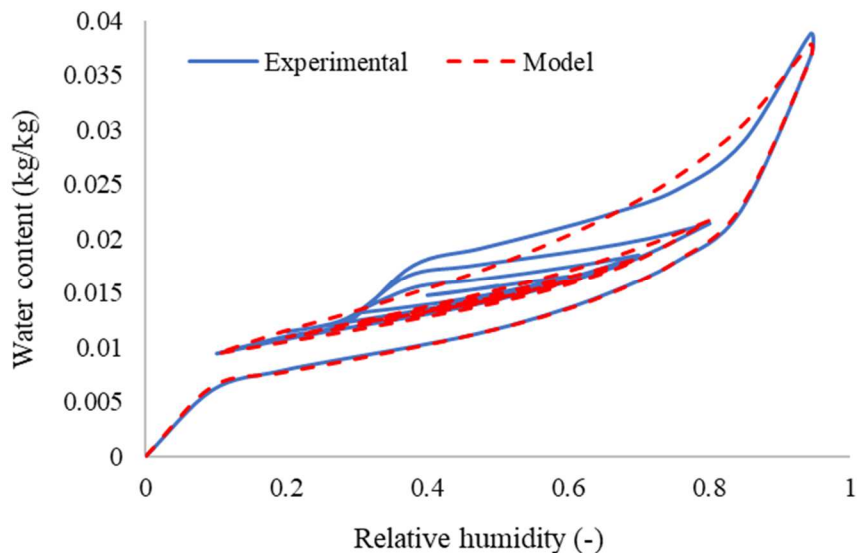


380

381 **Fig.9** Main and intermediate sorption isotherm curves of the polystyrene mortar

382 The intermediate curves represent the variations of water content of the material under
383 cyclic varying relative humidity. The hysteresis model developed by Carmeliet [39] should be
384 able to model the water content so that it can follow the same path. In the figure 10, the

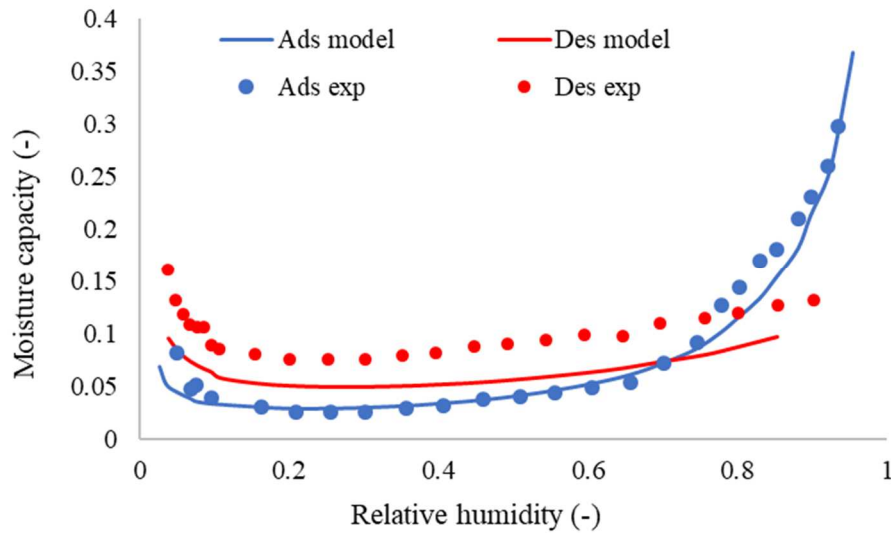
385 experimental and modelled intermediate curves are compared, and show a better adequacy in
386 adsorption phases. On the other hand, in the desorption phases, the modelled curves
387 underestimate the experimental curves and almost overlap. This is due to the sudden decrease
388 of water content in the main desorption curve between 30% and 40% of relative humidity.
389 Indeed, the sudden variation is very difficult model, and the modelled main desorption curve
390 tend to underestimate the experimental one. Therefore, all the following intermediate curves
391 are underestimating the water content values. Moreover, Carmeliet model ensures the closing
392 principle that helps avoiding pumping errors and each scanning adsorption and desorption
393 curve meet at the same value of water content.



394
395 **Fig.10** Experimental and modelled main and intermediate sorption curves of the polystyrene
396 mortar

397 The hysteresis model is also used to model the moisture storage capacity of the
398 material in order to evaluate its accuracy. Moisture storage capacity is defined as the
399 derivative of the water content in relation to the relative humidity; it can then be obtained
400 from the sorption curves. In order to verify the accuracy of the hysteresis model, modelled
401 moisture storage capacity of polystyrene mortar is compared to the experimental in figure 11.
402 During the adsorption phase, the modelled moisture capacity shows very good concordance

403 with the experimental curve, since the highest difference is only 8%. In desorption, the model
404 give less adequate results and display bigger differences up to 30%. However, the variations
405 of the modelled curves look like the experimental ones, and the model allows preserving the
406 shape of the experimental curve.



407

408 **Fig.11** Experimental and modelled moisture storage capacity of polystyrene mortar

409 **4.2. Water content evolution through time**

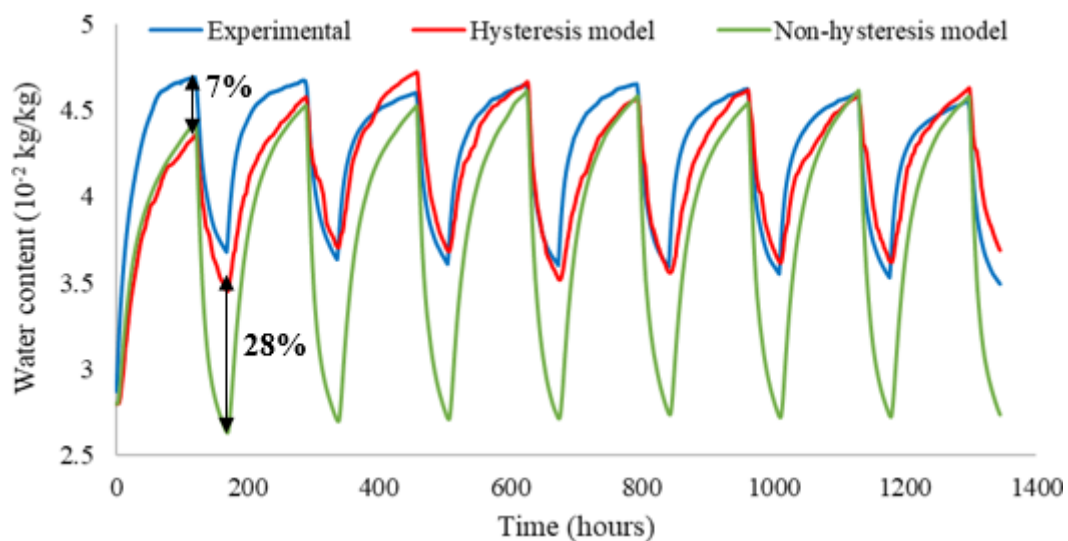
410 In the following, the experimental water content profiles inside the samples are presented.
411 They are compared to the numerical profiles obtained through simulations using the hysteresis
412 model presented in the previous parts. A non-hysteresis model will also be used in order to
413 assess the importance of the phenomenon consideration in the hygrothermal transfers
414 modelling in building materials. The results of each experimentation is presented apart from
415 the others below.

416 **4.2.1. Long lasting cycles at constant temperature**

417 Numerical and experimental results of the water content profiles in the samples submitted to
418 long lasting cycles at constant temperature are presented in figure 12. Using the non-
419 hysteresis model, the evolution of water content represents a curve below the experimental

420 results and underestimates the actual values. In the adsorption phase, the difference between
421 the experimental and simulated curves is relatively low, and the highest relative gap observed
422 is 5%. On the contrary, during desorption, the non-hysteresis model underestimates the real
423 water content values. The difference in this case is highly significant and the simulated values
424 show relative gaps reaching 28%.

425 The profiles obtained with the hysteresis model show a good adequacy with the experimental
426 results, except the first adsorption cycle where the difference is relatively high. Indeed the
427 numerical values of water content are lower than the experimental ones, and a 7% relative
428 difference is recorded at the peak of the first cycle. Concerning the remaining cycles, the
429 numerical curves are in good concordance with the experiments and the relative differences
430 do not exceed 2%.



431

432 **Fig.12** Experimental and numerical water content profiles in the first test

433 The discrepancy in the first cycle could result from a delay of the model, due to the initial
434 conditions. In fact, the material is initially conditioned at 60% of relative humidity, which
435 corresponds to a water content of 2.8% kg/kg before going through the first adsorption. In the
436 model, the initial water content put in the input parameters corresponds to that. Afterwards, at

437 the end of each desorption cycle, the sample has a water content of about 3.5% kg/kg.
438 Therefore, during humidification where the relative humidity is at 85%, it is easier for the
439 material to reach the maximum water content (4.7% kg/kg) when it is at 3.5% kg/kg than
440 when it is at its initial value. In reality, polystyrene mortar is not very hygroscopic, and so it
441 quickly reaches the maximum water content even when it is at the initial water content.

442 **4.2.2. Short lasting cycles at constant temperature**

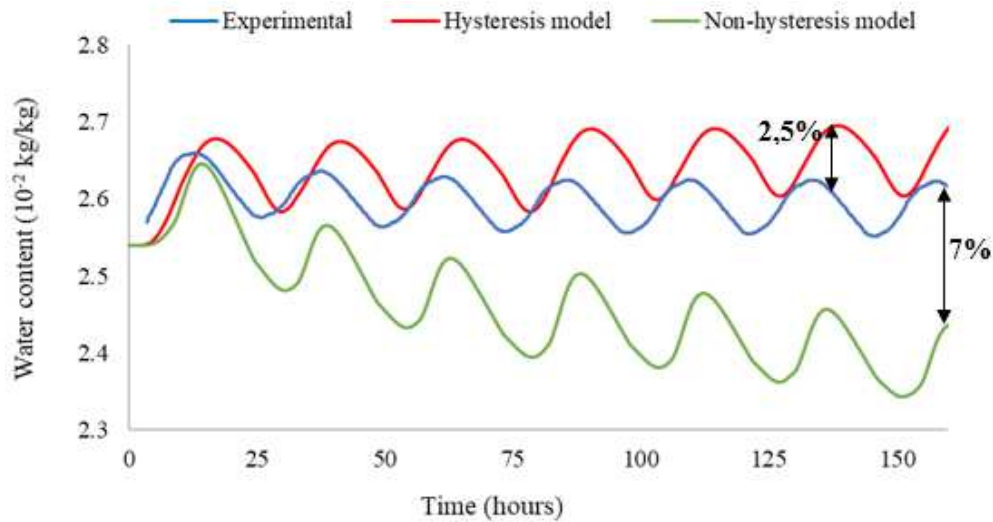
443 The second experiment consists of short lasting cycles at constant temperature, and the water
444 content profiles are presented in figure 13. The water content curve simulated with the non-
445 hysteresis model has the same shape as the experimental curve, and their amplitudes are
446 similar. The real water content values are underestimated since the numerical curve is below
447 the experimental, and the relative gap increases a little more with each cycle, until reaching a
448 maximum value of 7% in the last cycle.

449 Using a non-hysteresis model in simulating the hygrothermal behavior of building materials is
450 not a wise choice. Indeed, it is not advised to underestimate the water content in building
451 walls in hygrothermal transfer simulations, because of water accumulation that could degrade
452 the construction if not taken into consideration.

453 In a second time, the numerical curves acquired using the hysteresis model show the effect of
454 the sorption hysteresis phenomenon. This latter is less apparent in the experimental results
455 because of the drying period that is higher than the humidification. The numerical profiles
456 have the same amplitude as the experimental, but show a slight increase in time. However, the
457 displayed relative difference is only of 2.5% corresponding to barely 0.07% kg/kg, and the
458 simulated curves are in good agreement with the experimental.

459 The hysteresis model uses the main adsorption and desorption isotherm curves as input
460 parameters, which are based on equilibrium measurements. On the other hand, the

461 measurements in this test are carried out in dynamic regime, which may explain the
462 differences between the experimental and numerical results.



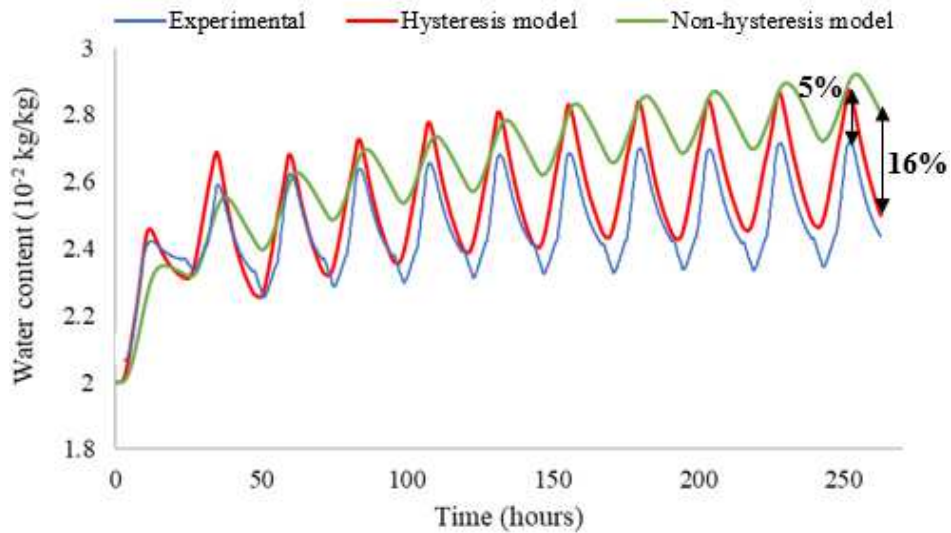
463

464 **Fig.13** Experimental and numerical water content profiles in the second test

465 Consequently, the water content profiles obtained with the hysteresis model have a better
466 concordance with the real water content profiles, in comparison with the profiles obtained
467 with the non-hysteresis model. The simulated curves have the same shape as the experimental
468 curves, as well as the same variations and amplitudes, and an admissible difference.

469 **4.2.3. Short lasting cycles at varying temperature**

470 The third experimentation is based on short lasting cycles at a varying temperature,
471 corresponding to the daily variations of temperature and relative humidity. As can be seen in
472 figure 14, the experimental curve shows a discrepancy in the first cycle, where the water
473 content is lower than in the others. This is due to a malfunctioning of the climatic chamber,
474 which did not secure the required temperature and relative humidity during the first cycle.
475 Given that the real climatic conditions recorded inside the chamber are used in the numerical
476 simulations, the simulated water content profiles display the same behavior in the first cycle.



477

478 **Fig.14** Experimental and numerical water content profiles in the third test

479 In this experimentation, the simulated water content curve using the non-hysteresis model is
 480 not located below the experimental curve, contrary to the two previous tests. In fact, the water
 481 content values are overestimated, and the high values obtained could be due to the varying
 482 temperature and its effect on moisture transfers. In addition to that, the amplitude of the
 483 simulated curve is significantly lower and corresponds to only 40% of the real one. The
 484 relative difference gradually increases as cycles progress, and attain a maximum value of
 485 16%.

486 The curve obtained using the hysteresis model shows a very good concordance with the
 487 experimental one. Although the water accumulation due to hysteresis is slightly greater in
 488 simulated curves, only a small difference is observed. Indeed, the highest relative gap is about
 489 5%, which can be considered as included in the precision range of the sensors. The hysteresis
 490 model also allows to maintain the shape and the amplitude of the experimental water content
 491 profiles, unlike the non-hysteresis model.

492 **5. Conclusion**

493 In this paper, we presented an experimental and numerical study of the water vapor
494 sorption hysteresis phenomenon in expanded polystyrene mortar. First, a coupled heat and
495 mass transfer model was presented allowing the sorption hysteresis consideration through the
496 physical model of Carmeliet. Afterwards, the experimental setup was presented, along with
497 the protocols and hygrothermal conditions. The experimental profiles were then compared to
498 the simulated ones in order to assess the influence of hysteresis consideration in hygrothermal
499 modelling of building materials.

500 The developed experimentations aim to highlight the sorption hysteresis phenomenon
501 via submitting the samples to multiple cyclic conditions, varying in temperature and relative
502 humidity. High precision sensors were inserted in the samples in order to record the water
503 content evolution during the time of the experiment. The experimental profiles were later
504 compared to simulated ones, obtained using the hysteresis model coupled to the hygrothermal
505 transfer model, and also a non-hysteresis model used to evaluate the influence of considering
506 hysteresis in numerical simulation.

507 The three different experimentations showed the same conclusion: Sorption hysteresis
508 consideration allows obtaining a better adequacy between simulated and experimental results.
509 In fact, the simulated curves using the hysteresis model had the same shape and amplitude as
510 the experimental ones, and the difference did not exceed 7%. On the other hand, the non-
511 hysteresis model showed numerical curves that either highly underestimated or overestimated
512 the real water content values. Moreover, their amplitude did not match the experimental one,
513 and the relative gaps were significantly important and reached 28%.

514 The water vapor sorption hysteresis phenomenon highly affects the hygrothermal
515 transfers in building materials, as it causes water accumulation in the pores. Its consideration
516 allows to a better apprehension of the real water content in porous materials and thus a better
517 understanding of the hygrothermal behavior of buildings.

518

519 **CRedit authorship contribution statement**

520 **Maroua Maaroufi:** Investigation, Methodology, Validation, Writing - original draft, Writing
521 - review & editing.

522 **Fares Bennai:** Validation, Writing - review & editing, Visualization.

523 **Rafik Belarbi:** Conceptualization, Writing - review & editing, Supervision, Validation.

524 **Kamilia Abahri:** Supervision, Validation.

525 **Declaration of Competing Interest**

526 The authors declare that they have no known competing financial interests or personal
527 relationships that could have appeared to influence the work reported in this paper.

528 **Acknowledgments**

529 The Region and the European Union support the project < CPER BATIMENT DURABLE.
530 Axis 2 MADUR Project: High-performance building materials with low environmental
531 impact, sustainable and resilient > within the framework of the « Operational Program
532 FEDER/FSE 2015-2020 » and Energy saving certificate program of the French Ministry of
533 Ecological and Solidarity Transition "SmartReno Support" 2019-2021.

534 **References**

535 [1] Mendes N., Winkelmann F.C., Lamberts R., Philippi P. C. (2003), Moisture effects on
536 conduction loads. *Energy and Buildings*, 35 (7):631-644

537 [2] Zhuang C., Wang S., Shan K. (2019). Adaptive full-range decoupled ventilation strategy
538 and air-conditioning systems for cleanrooms and buildings requiring strict humidity control
539 and their performance evaluation. *Energy*, 168:883-896

- 540 [3] Annala P. J., Lahdensivu J., Suonketo J., Pentti M., Vinha J. (2018). Need to repair
541 moisture- and mould damage in different structures in finnish public buildings. Journal of
542 Building Engineering, Volume 16:72-78
- 543 [4] John F. (2002). Moisture in buildings, ASHRAE J., 44 (15)
- 544 [5] Moon H.J., Ryu S.H., Kim J.T. (2014). The effect of moisture transportation on energy
545 efficiency and IAQ in residential buildings. Energy Build, 75:439-446
- 546 [6] Xu C., Li S., Zou K. (2019). Study of heat and moisture transfer in internal and external
547 wall insulation configurations. Journal of Building Engineering, Volume 24, 100724
- 548 [7] Zhang X., Künzle H. M., Zillig W., Mitterer C., Zhang X. (2016). A Fickian model for
549 temperature-dependent sorption hysteresis in hygrothermal modeling of wood materials,
550 International Journal of Heat and Mass Transfer 100:58–64
- 551 [8] Kerestecioglu A., Gu L. (1990). Theoretical and computational investigation of
552 simultaneous heat and moisture transfer in buildings: evaporation and condensation theory.
553 ASHRAE Transact. I:447-454
- 554 [9] Tariku F., Kumaran K., Fazio P. (2010). Integrated analysis of whole building heat, air
555 and moisture transfer. Int. J. Heat Mass Transf., 53:3111-3120
- 556 [10] Pedersen C. R. (1992). Prediction of moisture transfer in building constructions. Building
557 and Environment, 27 (3):387-397
- 558 [11] Bennai F, Abahri K, Belarbi R (2020) “Contribution to the Modelling of Coupled Heat
559 and Mass Transfers on 3D Real Structure of Heterogeneous Building Materials: Application
560 to Hemp Concrete”. Transp Porous Med 133:333–356

- 561 [12] Bennai F, Abahri K, Belarbi R, Tahakourt A (2016) “Periodic homogenization for heat,
562 air, and moisture transfer of porous building materials”. *Numerical Heat Transfer, Part B:
563 Fundamentals* 70:420–440
- 564 [13] J. Eitelberger and K. Hofstetter, “Prediction of transport properties of wood below the
565 fiber saturation point – a multiscale homogenization approach and its experimental validation:
566 Part i: Thermal conductivity”, *Composites Science and Technology* 71 (2011), no. 2, 134–
567 144.
- 568 [14] M. Sejnoha, J. Sykora, J. Vorel, L. Kucikova, J. Antos, J. Pokorny, and Z. Pavlik,
569 “Moisture induced strains in spruce from homogenization and transient moisture transport
570 analysis”, *Computers & Structures* 220 (2019), 114–130.
- 571 [15] Pedersen C.R. (1990). *Combined Heat and Moisture Transfer in Building Constructions*.
572 Technical University of Denmark
- 573 [16] Maaroufi M., Abahri K., Bennai F., Belarbi R. (2019). Moisture transfer modelling in
574 polystyrene mortar with consideration of sorption hysteresis. *E3S Web Conf.*, Volume 128
- 575 [17] Pedersen C.R. (1990). Transient calculation on moisture migration using a simplified
576 description of hysteresis in sorption isotherms. *Proceedings of 2nd Nordic Symposium on
577 Building Physics*, Trondheim, Norway
- 578 [18] Samri D. (2008). *Analyse physique et caractérisation hygrothermique des matériaux de
579 construction: approche expérimentale et modélisation numérique*. Phd thesis, Ecole Nationale
580 des Travaux Publics de l'Etat, France
- 581 [19] Schiller P., Wahab M., Bier T., Waida S., Mögel H.J. (2015). Capillary Forces and
582 Sorption Hysteresis of Cement Pastes with Small Slit Pores. *5th International Biennial*

583 Conference on Ultrafine Grained and Nanostructured Materials UFGNSM15, Procedia
584 materials science

585 [20] Zhang Z. (2013). Modelling of sorption hysteresis and its effect on moisture transport
586 within cementitious materials. Phd thesis, University Paris-Est, France

587 [21] Ait Oumeziane Y. (2013). Evaluation des performances hygrothermiques d'une paroi par
588 simulation numérique : application aux parois en béton de chanvre. Phd thesis, University of
589 Rennes, France

590 [22] Rode, C. (2005). Moisture Buffering of Building Materials. Report R-126, Technical
591 University of Denmark

592 [23] Lelièvre D. (2015). Simulation numérique des transferts de chaleur et d'humidité dans
593 une paroi multicouche de bâtiment en matériaux biosourcés. Phd thesis, European university
594 of Bretagne, France

595 [24] Schiller P., Wahab M., Bier T., Mögel H.-J. (2019). A model for sorption hysteresis in
596 hardened cement paste. Cement and Concrete Research, Volume 123, 105760

597 [25] Jiang Z., Xi Y., Gu X., Huang Q., Zhang W. (2019). Modelling of water vapour sorption
598 hysteresis of cement-based materials based on pore size distribution. Cement and Concrete
599 Research, Volume 115:8-19

600 [26] Bennai F., Issaadi N., Abahri K., Belarbi R., Tahakourt A. (2018). Experimental
601 characterization of thermal and hygric properties of hemp concrete with consideration of the
602 material age evolution. Heat and Mass Transfer volume 54:1189–1197

603 [27] Arfvidsson J. and Claesson J. (2000). Isothermal moisture flow in building materials:
604 modelling, measurements and calculations based on kirchhoff's potential. Building and
605 Environment 35:519-536

- 606 [28] Arfvidsson J. (1999). Moisture penetration depth for periodically varying relative
607 humidity at the boundary. *Nordic Journal of Building Physics* 2:75-80
- 608 [29] Derluyn H., Derome D., Carmeliet J., Stora E. and Barbarulo R. (2012). Hysteretic
609 moisture behavior of concrete: Modelling and analysis. *Cement and Concrete Research*
610 42:1379-1388
- 611 [30] A.V. Luikov, "Heat and Mass Transfer in Capillary-porous Bodies", *Advances in heat*
612 *transfer*, Volume 1, 1964, Pages 123-184
- 613 [31] M.Y. Ferroukhi, R. Djedjig, K. Limam, R. Belarbi, "Hygrothermal behavior modeling of
614 the hygroscopic envelopes of buildings: A dynamic co-simulation approach", *Building*
615 *Simulation*, October 2016, Volume 9, Issue 5, pp 501-512.
- 616 [32] H. Janssen, "Thermal diffusion of water vapour in porous materials: Fact or fiction?"
617 March 2011, *International Journal of Heat and Mass Transfer* 54(7-8):1548-1562
- 618 [33] A. Trabelsi, R. Belarbi, K. Abahri, M. Qin Reply on the comments regarding the paper:
619 "Assessment of temperature gradient effects on moisture transfer through thermogradient
620 coefficient", *Building Simulation: An International Journal*, Volume 6 (1), 2013, pp. 109-110.
- 621 [34] Koronthalyova O. (2011). Moisture storage capacity and microstructure of ceramic brick
622 and autoclaved aerated concrete. *Construction and Building Materials*, Volume 25, Issue
623 2:879-885
- 624 [35] Kunzel H.M. (1995). Simultaneous heat and moisture transport in building components:
625 one- and two-dimensional calculation using simple parameters. *Fraunhofer IRB Verlag*
626 *Stuttgart* ISBN 3-8167-4103-7, Allemagne

- 627 [36] Colinart T., Lelièvre D., Glouannec P. (2014). Influence de l’hystérésis sur le
628 comportement hygrothermique d’un enduit de finition intérieure biosourcé. Conférence
629 IBPSA France
- 630 [37] NF EN 12667, Thermal performance of building materials and products - Determination
631 of thermal resistance by means of guarded hot plate and heat flow meter methods - Products
632 of high and medium thermal resistance
- 633 [38] AFNOR, NF EN ISO 12572, “Hygrothermal performance of building materials and
634 products — Determination of water vapor transmission properties”, 2001.
- 635 [39] Carmeliet J., DeWit M., Janssen H. (2005). Hysteresis and moisture buffering of wood.
636 Proceedings of the Nordic Symposium on Building Physics, Iceland, pp 55–62
- 637 [40] Mualem Y. (1974). A conceptual model of hysteresis. *Water Resources Research*,
638 Volume 10 (3):514-520
- 639 [41] Mualem Y. (1973). Modified approach to capillary hysteresis based on a similarity
640 hypothesis. *Water Resources Research* (9):1324-1331
- 641 [42] Huang H., Tan Y., Liu C. & Chen C. (2005). A novel hysteresis model in unsaturated
642 soil. *Hydrological Processes* 19:1653-1665
- 643 [43] Werner A. D., Lockington D. A. (2006). Artificial pumping errors in the kool-parker
644 scaling model of soil moisture hysteresis. *Journal of Hydrology* 325:118-133
- 645 [44] Maaroufi M., Abahri K., El Hachem C., Belarbi R. (2018). Characterization of EPS
646 lightweight concrete microstructure by X-ray tomography with consideration of thermal
647 variations. *Construction and Building Materials* 178:339–348

- 648 [45] Maaroufi M., Younsi A., Nouviaire A., Belarbi R. (2018). Influence of recycled
649 polystyrene beads on cement paste properties. 2nd International Congress on Materials &
650 Structural Stability (CMSS-2017), MATEC Web of Conference, Volume 149
- 651 [46] ASTM Annual book of standards, Standard test method for water vapor transmission of
652 materials, Philadelphia, 2005
- 653 [47] NF EN 12667, Performance thermique des matériaux et produits pour le bâtiment -
654 Détermination de la résistance thermique par la méthode de la plaque chaude gardée et la
655 méthode fluxmétrique – Produits de haute et moyenne résistance thermique, 2001